

# Three-dimensional Moiré Crystal

Ce Wang,<sup>1</sup> Chao Gao,<sup>2,3,\*</sup> Jing Zhang,<sup>4,5</sup> Hui Zhai,<sup>6,5</sup> and Zhe-Yu Shi<sup>7,†</sup>

<sup>1</sup>*School of Physics Science and Engineering, Tongji University, Shanghai, 200092, China*

<sup>2</sup>*Department of Physics, Zhejiang Normal University, Jinhua, 321004, China*

<sup>3</sup>*Key Laboratory of Optical Information Detection and Display Technology of Zhejiang, Zhejiang Normal University, Jinhua, 321004, China*

<sup>4</sup>*State Key Laboratory of Quantum Optics and Quantum Optics Devices, Institute of Opto-Electronics, Collaborative Innovation Center of Extreme Optics, Shanxi University, Taiyuan, P. R. China*

<sup>5</sup>*Hefei National Laboratory, Hefei 230088, China*

<sup>6</sup>*Institute for Advanced Study, Tsinghua University, Beijing, 100084, China*

<sup>7</sup>*State Key Laboratory of Precision Spectroscopy, East China Normal University, Shanghai 200062, China*

(Dated: May 1, 2024)

The work intends to extend the moiré physics to three dimensions. Three-dimensional moiré patterns can be realized in ultracold atomic gases by coupling two spin states in spin-dependent optical lattices with a relative twist, a structure currently unachievable in solid-state materials. We give the commensurate conditions under which the three-dimensional moiré pattern features a periodic structure, termed a *three-dimensional moiré crystal*. We emphasize a key distinction of three-dimensional moiré physics: in three dimensions, the twist operation generically does not commute with the rotational symmetry of the original lattice, unlike in two dimensions, where these two always commute. Consequently, the moiré crystal can exhibit a crystalline structure that differs from the original underlying lattice. We demonstrate that twisting a simple cubic lattice can generate various crystal structures. This capability of altering crystal structures by twisting offers a broad range of tunability for three-dimensional band structures.

Large-scale moiré patterns emerge when two identical two-dimensional structures are overlaid with an offset. During recent years, studies on double-layered two-dimensional materials, such as twisted bilayer graphenes [1–6], twisted transition metal dichalcogenides [7, 8] and twisted cuprates [9, 10], reveal that moiré patterns can substantially alter the electronic properties of the material. Many extraordinary phenomena, including flat bands [11, 12], unconventional superconductivity [13–15], ferromagnetism [16, 17], fractional Chern insulator [18–22] and fractional quantum anomalous Hall effect [23–26], have been predicted and discovered through creating moiré patterns in two-dimensional materials by twisting. The growing interest in twisted bilayer materials has developed a new field in condensed matter physics, known as twistrionics [27, 28].

The impact of twistrionics goes beyond condensed matter physics. For instance, moiré superlattice has been achieved in photonic crystals [29–32] and optical lattices [33], paving the way for studying moiré physics in electromagnetic waves and ultracold atoms. Remarkably, the recent experimental realization of a two-dimensional moiré lattice in ultracold atomic gases utilizes the two internal states (spins) of atoms instead of two spatially separated layers [33]. In the experiment, ultracold <sup>87</sup>Rb atoms are loaded in two spin-dependent two-dimensional optical lattices with a relative twisted angle. The wavelengths of these two optical lattices are carefully selected such that each lattice only couples to one of the two spin states of a <sup>87</sup>Rb atom and is transparent to the other spin component. Therefore, although atoms with differ-

ent spins coexist in the same space, their lattice potentials can be viewed as two independent layers, and an external microwave-induced coupling between the two spin states can play the role of inter-layer tunneling. In this way, a moiré superlattice can be realized in an optical lattice setting, leading to an intriguing new phase observed between the conventional superfluid and Mott insulator transition [33].

This letter proposes that this scheme of realizing moiré physics in ultracold atoms can be generalized to three dimensions. The flexibility in ultracold atom apparatus allows twisting two sets of spin-dependent three-dimensional optical lattices along a generic axis  $\mathbf{L}$  (not any of the principle axes of the original lattice) at a generic angle  $\theta$ . Hence, it can create a *three-dimensional moiré crystal* when  $\mathbf{L}$  and  $\theta$  satisfy the commensurate condition discussed below. This generalization promotes moiré physics from two dimensions to three, presenting numerous new possibilities and opening up a new avenue in twistrionics.

Here, we highlight a fundamental difference between the moiré physics in two and three dimensions. The difference stems from the non-abelian nature of the SO(3) rotation group, as opposed to the abelian SO(2) group. A two-dimensional twist, i.e., an element in SO(2), always commutes with the rotation symmetry of the original two-dimensional lattice, such as the  $C_4$  rotation of a square lattice. Consequently, the moiré patterns of twisted bilayer square lattices always retain the exact  $C_4$  symmetry. In contrast, a three-dimensional twist belonging to the non-abelian SO(3) group generally does

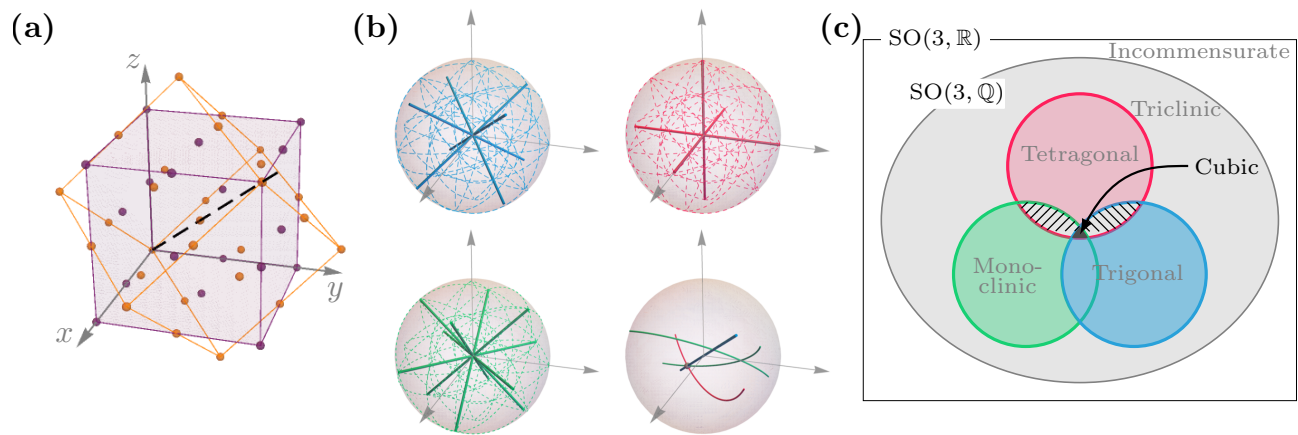


FIG. 1. (a) Schematic of an example of a three-dimensional moiré crystal. Two sets of cubic optical lattices, represented by the purple and yellow dots, are twisted along the body diagonal (111) direction (dashed line). (b) Three-dimensional twists under which the moiré crystal exhibits different rotational symmetry. Each rotation in  $SO(3)$  is represented by a point  $\mathbf{r} = |\mathbf{r}|\hat{\mathbf{e}}_r$  within a ball of radius  $\pi$ . Here,  $\hat{\mathbf{e}}_r$  represents the twisting axes, and  $|\mathbf{r}|$  is the twist angle. The blue, red, and green lines indicate twists where the moiré crystals have  $C_3$ ,  $C_4$ , or  $C_2$  symmetry, respectively. The solid lines are positioned along the cubic lattice's symmetry axes. Twists belong to these lines thus preserve the corresponding rotational symmetries. Additionally, twists represented by the dashed curves also lead to rotationally symmetric moiré crystals. This is due to every twist  $R$  on a dashed curve may be transformed into a twist  $R'$  on a solid line by  $R = R'g$ , where  $g \in O$ . The lower right panel illustrates that the green line can intersect with the blue line, and these three lines can intersect at a single point. Twists represented by these intersection points possess multiple rotational symmetries. (c) The Venn diagram describing the crystal systems of different twists is presented in (b). The red, green, and blue areas represent the Tetragonal, Monoclinic, and Trigonal crystal systems of moiré crystal generated by the respective twists in (b). The black area represents the cubic moiré crystal generated by the intersection of these lines with different colors. Areas marked by dashed lines are empty sets. The grey area represents a Triclinic crystal system with no rotational symmetry.

not commute with the rotation symmetry of the original three-dimensional lattice. As a result, a three-dimensional twist can disrupt the rotational symmetry of the original lattice, resulting in a distinct point group symmetry for the three-dimensional moiré crystal. This property allows a wide range of crystal structures to be generated by twisting the same lattice. It is worth mentioning that there have been previous studies on the moiré effect on three-dimensional solid-state systems [34–37]. However, these studies focus on systems of stacked multiple layers of twisted two-dimensional materials. Thus, accessible rotations in these systems are intrinsically two-dimensional and are different from the moiré crystals considered in this work.

*Physical Model.* A three-dimensional moiré crystal can be described by the following Hamiltonian of ultracold atoms with two spin components

$$H = \begin{pmatrix} \frac{\mathbf{p}^2}{2m} + V_A + \frac{\delta}{2} & \Omega \\ \Omega & \frac{\mathbf{p}^2}{2m} + V_B - \frac{\delta}{2} \end{pmatrix}, \quad (1)$$

where  $m$  is the mass of atoms and  $\mathbf{p}$  is the momentum,  $\Omega$  represents the coupling between two spin states with a detuning  $\delta$ , and  $V_{A,B}$  are the optical lattice potentials for the two spin states, respectively. For illustrative purposes, we consider a three-dimensional cubic lattice,

where  $V_A(\mathbf{r})$  is written as

$$V_A(\mathbf{r}) = -\frac{V}{4} [\cos^2(\pi x) + \cos^2(\pi y) + \cos^2(\pi z)]. \quad (2)$$

Here,  $V$  stands for the lattice depth, and the recoil momentum has been taken to be  $\pi$  for simplicity. The optical lattice potential  $V_B(\mathbf{r})$  is twisted with respect to  $V_A(\mathbf{r})$  by a three-dimensional rotation. This is characterized by a rotation matrix  $R \in SO(3)$  and a displacement  $\mathbf{d} \in \mathbb{R}^3$  as follows:

$$V_B(R\mathbf{r} + \mathbf{d}) = V_A(\mathbf{r}). \quad (3)$$

An example of the three-dimensional twisted moiré crystals is illustrated in Fig. 1(a).

*Commensurate Condition.* Similar to the two-dimensional moiré systems, the moiré crystal appears only when the rotation  $R$  satisfies certain commensurate conditions, presented by the following theorem.

**Theorem.** *The moiré pattern formed by overlapping two cubic lattices  $V_A(\mathbf{r})$  and  $V_B(\mathbf{r})$  forms a three-dimensional periodic lattice structure if and only if  $R \in SO(3, \mathbb{Q})$ .*

Here,  $SO(3, \mathbb{Q})$  is the set of all three-dimensional special orthogonal matrices with all entries being rational numbers [38]. In the supplementary material, we show that every rotation matrix  $R \in SO(3, \mathbb{Q})$  can be uniquely

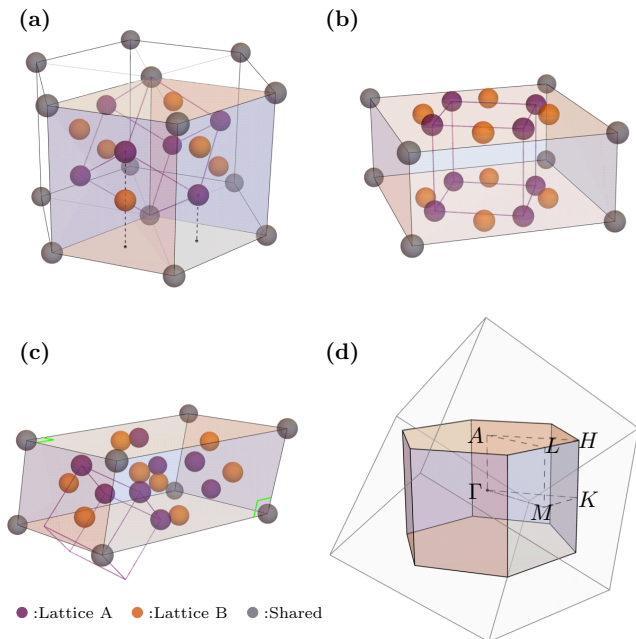


FIG. 2. (a-c) Lattice structures of twisted cubic lattices with different twisting axes  $\mathbf{L}$  and twisting angle  $\theta$ .  $\mathbf{L} = (1, 1, 1)$  and  $\theta = \pi/3$  with  $(m, n) = (3, 1)$  (a);  $\mathbf{L} = (0, 0, 1)$  and  $\theta = \arccos \frac{3}{5}$  with  $(m, n) = (2, 1)$  (b);  $\mathbf{L} = (1, 1, 0)$  and  $\theta = \arccos \frac{7}{9}$  with  $(m, n) = (4, 1)$  (c). They belong to the Trigonal, Tetragonal, and Monoclinic crystal systems. The blue, red, and gray dots represent the lattice sites of lattice A, lattice B, and those shared by both lattices. The unit cell is denoted by the shaded prism. (d) The first Brillouin zone (shaded hexagonal prism) and high symmetry points for the reciprocal lattice of the moiré crystal are presented in (a). The cube formed by the black edges represents the first Brillouin zone of the original cubic lattice A.

parametrized by the axis of rotation  $\mathbf{L} \equiv (l_1, l_2, l_3)$  and the rotation angle [39]

$$\theta = \arccos \frac{m^2 - n^2 |\mathbf{L}|^2}{m^2 + n^2 |\mathbf{L}|^2}. \quad (4)$$

Here  $(l_1, l_2, l_3)$  are three integers with  $\gcd(l_1, l_2, l_3) = 1$ , and  $(m, n)$  are two integers with  $\gcd(m, n) = 1$ , where  $\gcd$  stands for the greatest common divisor. Note that if we take the rotation axis  $\mathbf{L} = (0, 0, 1)$ , Eq. (4) becomes  $\theta = \arccos \frac{m^2 - n^2}{m^2 + n^2}$ , which coincides the commensurate condition for a twisted bilayer square lattice [33, 40].

*Proof of the Theorem.* Note that all the lattice vectors of  $V_A$  form a three-dimensional Bravais lattice  $\mathbb{Z}^3$ , i.e.  $V_A(\mathbf{r} + \mathbf{a}) = V_A(\mathbf{r})$  for all  $\mathbf{r}$  if and only if  $\mathbf{a} \in \mathbb{Z}^3$ . Similarly, the lattice vectors of  $V_B$  form the set  $R\mathbb{Z}^3 \equiv \{R\mathbf{a} | \mathbf{a} \in \mathbb{Z}^3\}$ . One thus concludes that a vector  $\mathbf{u}$  is a period of the moiré pattern if and only if  $\mathbf{u} \in \mathbb{Z}^3 \cap R\mathbb{Z}^3$ . Furthermore, the moiré pattern forms a three-dimensional lattice if and only if  $\mathbb{Z}^3 \cap R\mathbb{Z}^3$  is a three-dimensional Bravais lattice.

To prove the theorem, we first show that if the rotation  $R \in \text{SO}(3, \mathbb{Q})$ , then  $\mathbb{Z}^3 \cap R\mathbb{Z}^3$  is a three-dimensional Bra-

vais lattice. Consider vectors  $R\hat{e}_1$ ,  $R\hat{e}_2$ , and  $R\hat{e}_3$ , where  $\hat{e}_1 = (1, 0, 0)^T$ ,  $\hat{e}_2 = (0, 1, 0)^T$ , and  $\hat{e}_3 = (0, 0, 1)^T$ . These three vectors are linearly independent and have rational components if  $R \in \text{SO}(3, \mathbb{Q})$ . One can then find integers  $n_i$ , such that all components of  $n_i \cdot R\hat{e}_i$  are integers for each  $i = 1, 2, 3$ . This demonstrates that there exist three linearly independent vectors  $n_i \cdot R\hat{e}_i \in \mathbb{Z}^3 \cap R\mathbb{Z}^3$ ,  $i = 1, 2, 3$ , and hence  $\mathbb{Z}^3 \cap R\mathbb{Z}^3$  is a three-dimensional Bravais lattice.

To prove the converse, we note that if  $\mathbb{Z}^3 \cap R\mathbb{Z}^3$  is a three-dimensional Bravais lattice, there must exist three linearly independent integer vectors  $\mathbf{u}_1, \mathbf{u}_2, \mathbf{u}_3 \in \mathbb{Z}^3 \cap R\mathbb{Z}^3$ . Since  $\mathbf{u}_1, \mathbf{u}_2, \mathbf{u}_3 \in R\mathbb{Z}^3$ , there exist linearly independent integer vectors  $\mathbf{v}_1, \mathbf{v}_2, \mathbf{v}_3$  such that  $R(\mathbf{v}_1, \mathbf{v}_2, \mathbf{v}_3) = (\mathbf{u}_1, \mathbf{u}_2, \mathbf{u}_3)$ . By writing  $U = (\mathbf{u}_1, \mathbf{u}_2, \mathbf{u}_3)$  and  $V = (\mathbf{v}_1, \mathbf{v}_2, \mathbf{v}_3)$ , we thus have  $R = UV^{-1} \in \text{SO}(3, \mathbb{Q})$ . This completes the proof.

The above proof shows that the periodicity of a moiré crystal is determined solely by the twist  $R$ , i.e. it is not affected by the displacement  $\mathbf{d}$ . Furthermore, it also provides an algorithm for calculating the unit cells and unit vectors of a three-dimensional moiré crystal. Note that a vector  $\mathbf{u} \in \mathbb{Z}^3$  is a lattice vector if and only if there exists  $\mathbf{v} \in \mathbb{Z}^3$  such that  $R\mathbf{u} - \mathbf{v} = 0$ . This equation can be viewed as a set of linear Diophantine equations for six integer variables  $u_i, v_i$ ,  $i = 1, 2, 3$ , where  $u_i$  and  $v_i$  are the  $i$ th components of  $\mathbf{u}$  and  $\mathbf{v}$ . Given that  $R \in \text{SO}(3, \mathbb{Q})$ , it can be shown that every solution  $(\mathbf{u}, \mathbf{v})^T$  can be uniquely expressed as an integer linear combination of three solutions  $(\mathbf{u}_1, \mathbf{v}_1)^T$ ,  $(\mathbf{u}_2, \mathbf{v}_2)^T$  and  $(\mathbf{u}_3, \mathbf{v}_3)^T$ . Therefore,  $\mathbf{u}_1, \mathbf{u}_2, \mathbf{u}_3$  span the Bravais lattice  $\mathbb{Z}^3 \cap R\mathbb{Z}^3$  and can be chosen as the unit lattice vectors of the three-dimensional moiré crystal [39].

*Symmetry of Moiré Crystal.* We now examine the crystal structures of moiré crystal by investigating its chiral point group, i.e., the set of all the proper rotational symmetries of the lattice. For simplicity, from this point forward, we will focus on the case where the displacement  $\mathbf{d} = 0$ , unless specified otherwise.

It is well known that the rotational symmetry of a cubic lattice  $V_A$  is described by the chiral octahedral group  $O$ . This group consists of 24 rotations [41]. As  $V_B$  is a lattice generated by twisting  $V_A$  by a rotation  $R$ , its chiral point group is then  $ROR^{-1} \equiv \{RO_iR^{-1} | O_i \in O\}$ . Consequently, the chiral point group of the moiré crystal can be directly inferred as  $O \cap ROR^{-1}$ .

At this point, we can further elaborate on the distinction between the moiré lattice in two and three dimensions. In two dimensions, because the rotation group  $\text{SO}(2, \mathbb{R})$  is abelian, one has  $RgR^{-1} \equiv g$  for any  $g, R \in \text{SO}(2, \mathbb{R})$ . Therefore,  $O \cap ROR^{-1} \equiv O$  and the moiré lattice always maintain the same rotational symmetry as the original lattice. In three dimensions, however, one generically has  $RgR^{-1} \neq g$  because of the non-abelian nature of  $\text{SO}(3, \mathbb{R})$ . The chiral point group of a three-dimensional moiré crystal is thus different from that of the original

lattice and, more crucially, can be tuned by choosing an appropriate twist  $R$ . In Fig. 1(b), we illustrate different classes of twists that lead to different rotation symmetries of the moiré crystals. We use a three-dimensional ball with radius  $\pi$  to represent all SO(3) rotation symmetry, where the direction  $\hat{e}_r$  of a given point denotes its rotation axis and the length  $|\mathbf{r}|$  denotes its rotation angle.

In the first plot, the blue lines represent all the twists that can lead to a  $C_3$  symmetric moiré crystal belonging to the Trigonal crystal system. Note that the blue solid lines contain all the rotations along the body diagonals such as the (1, 1, 1) direction. As these body diagonals are the  $C_3$  axes of the original cubic lattice  $V_A$ , any rotation along one of these axes preserves the corresponding rotation symmetry. However, these rotations do not cover all the twists resulting in  $C_3$  symmetry. We emphasize that two rotations  $R$  and  $R'$  should yield the same moiré crystal if  $R = R'g$  for some  $g$  belonging to the chiral octahedral group, i.e. the rotation symmetries of  $V_A$ . This equivalence generates other dashed blue lines in the plot which cover all the rotations leading to moiré crystals with  $C_3$  symmetry.

Similarly, in the other two plots of Fig. 1(b), we illustrate the twists that result in a moiré crystal with  $C_4$  symmetry (red lines) belonging to Tetragonal crystal system, or  $C_2$  symmetry (green lines) belonging to Monoclinic crystal system, assuming no other rotational symmetry exists. The last plot of Fig. 1(b) gives examples of how a green line could intersect with a blue line, where the intersection points denote a twist resulting in both  $C_3$  and  $C_2$  symmetry, also belonging to the Trigonal crystal system. Moreover, three lines of different colors can also intersect at the same point, representing a twist that can recover the cubic symmetry. Finally, other twists in SO(3,  $\mathbb{Q}$ ) but does not belong to the lines in Fig. 1(b) lead to moiré crystal with no rotational symmetry, belonging to the Triclinic class.

The classification of the moiré crystal systems is shown in Fig. 1(c) by the Venn diagram. Notably, a rich set of crystal structures, i.e., five out of a total of seven possible crystal systems in three dimensions, emerge through twisting two simple cubic lattices. In Fig. 2 we present three examples of different moiré crystal belonging to Trigonal, Tetragonal and Monoclinic crystal systems, respectively. The grey points denote the lattice sites shared by A and B lattices, clearly illustrating unit cells with diverse geometries.

**Band Structures.** The ability to control the crystalline symmetry through three-dimensional twists offers increased flexibility for engineering band dispersion. Here, as a first demonstration of such tunability in three dimensions, we focus on a specific rotation parametrized by twisting along  $\mathbf{L} = (1, 1, 1)$  by  $\theta = \pi/3$ . The real space moiré crystal structure is shown in Fig. 2(a), and its moiré Brillouin zone is depicted in Fig. 2(d). This is

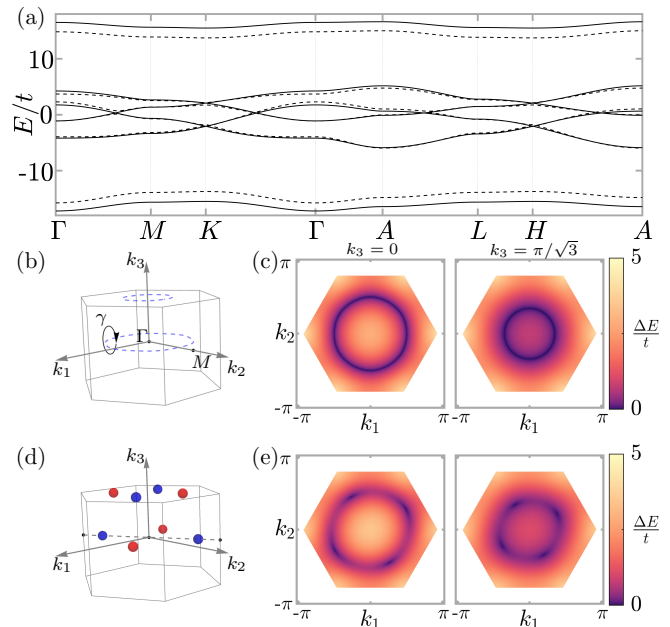


FIG. 3. (a) Band structures of the moiré crystal with twisting axes  $\mathbf{L} = (1, 1, 1)$  and twisting angle  $\theta = \pi/3$  with  $(m, n) = (3, 1)$ , whose real space structure is shown in Fig. 2(a). The displacements between  $V_A$  and  $V_B$  are  $\mathbf{d} = (0, 0, 0)$  for solid lines, and  $\mathbf{d} = (0, 0.1, -0.1)$  for dashed lines. The calculations are based on tight-binding approximation for Hamiltonian (1) with parameters  $V = 6\pi^2/(2m)$ ,  $\Omega = \pi^2/(2m)$  and  $\delta = 0$ . (b,d) Schematic plots showing two topological nodal lines for displacement  $\mathbf{d} = (0, 0, 0)$  (b) and eight Weyl points for displacement  $\mathbf{d} = (0, 0.1, -0.1)$  (d). The blue/red points indicate the positions for Weyl points with Chern number  $+1/-1$ . (c,e) Band gaps  $E_4(\mathbf{k}) - E_3(\mathbf{k})$  for displacement  $\mathbf{d} = (0, 0, 0)$  (c) and  $\mathbf{d} = (0, 0.1, -0.1)$  (e). Left:  $k_3 = 0$  plane; Right:  $k_3 = \pi/\sqrt{3}$  plane. Note that the dark spots denote the positions of the gapless points.

reminiscent of the Brillouin zone of many materials with symmetry-protected nodal lines or nodal points [42–46]. Therefore, it inspires us to examine the topological feature in this moiré crystal.

In Fig. 3, we plot the band structures of this moiré crystal under a tight-binding approximation [47]. Interestingly, it is discovered that the dispersion can support nontrivial gapless lines between the third and the fourth bands [39], as shown in Fig. 3 (b) and (c). These two gapless lines in  $k_3 = 0$  and  $k_3 = \pi/\sqrt{3}$  planes are topological nodal lines [48–52] protected by either the  $\mathcal{PT}$  symmetry or the  $\mathcal{M}\sigma_x$  symmetry simultaneously. Here,  $\mathcal{P}$  represents the inversion against the origin,  $\mathcal{T}$  represents the (spinless) time reversal operation,  $\mathcal{M}$  stands for the reflection against the plane perpendicular to the body diagonal (111) direction, and  $\sigma_x$  is the spin-flip operation for the two hyperfine spins. Both symmetries are maintained when  $\mathbf{d} = 0$ . When we introduce a finite perturbation in  $\mathbf{d}$ , e.g. along the (0, 1, -1) direction, both

two symmetries are simultaneously broken, which partially gaps the topological nodal lines and results in four pairs of gapless Weyl points [39, 53, 54], as shown in Fig. 3 (d) and (e). These Weyl points all carry nonvanishing Chern numbers with  $C = \pm 1$ , suggesting they are stable against perturbations that preserve the lattice translation symmetries.

*Conclusion and Outlook.* In summary, we propose to generalize the moiré physics to three dimensions. We present the commensurate condition for the moiré crystal and highlight that different crystal structures of the moiré pattern can be realized by twisting the same cubic lattice along different axes and angles. The specific features of three-dimensional moiré lattices will bring many opportunities for future research.

Firstly, the complexity of the three-dimensional rotation group allows more flexible band engineering, which can lead to non-trivial band topologies or flat bands. In this work, we have shown the example of generating topological nodal lines and Weyl points through a three-dimensional twist. Yet, given the extensive parameter space of the  $SO(3, \mathbb{Q})$  group, more systematic studies of band structures are required for future investigations. Secondly, two-dimensional moiré systems can exhibit a variety of highly non-trivial correlation effects by introducing interactions [6, 33, 55–59]. Similar or even more sophisticated correlation effects could occur in three dimensions. Thirdly, we have focused on commensurate crystals, while incommensurate twists can also reveal intriguing physics in three dimensions. Finally, we have discussed the potential for realizing a three-dimensional moiré crystal in ultracold atoms, and a similar realization may also be possible in photonic systems [60–62].

*Acknowledgement.* We thank Biao Lian, Zhong Wang, Zengming Meng, Jie Ren, Zhiwei Guo, Yizhou Liu, and Xingze Qiu for inspiring discussion. This work is supported by the National Natural Science Foundation of China (NSFC) under Grant Nos. 12204352 (CW), 10274342 (CG), 12034011 (JZ), U23A6004 (JZ and HZ), 12004115 (ZYS), the Innovation Program for Quantum Science and Technology under Grant Nos. 2021ZD0302003 (JZ), 2021ZD0302005 (HZ), the National Key R&D Program of China 2023YFA1406702 (HZ), and the XPLOER Prize (JZ and HZ), the Natural Science Foundation of Zhejiang Province, China under Grant Nos. LR22A040001 (CG) and LY21A040004 (CG).

\* gaochao@zjnu.edu.cn

† zyshi@jps.ecnu.edu.cn

- [1] Y. Cao, V. Fatemi, A. Demir, S. Fang, S. L. Tomarken, J. Y. Luo, J. D. Sanchez-Yamagishi, K. Watanabe, T. Taniguchi, E. Kaxiras, R. C. Ashoori, and P. Jarillo-Herrero, Correlated insulator behaviour at half-filling in magic-angle graphene superlattices, *Nature* **556**, 80 (2018).
- [2] Y. Cao, V. Fatemi, S. Fang, K. Watanabe, T. Taniguchi, E. Kaxiras, and P. Jarillo-Herrero, Unconventional superconductivity in magic-angle graphene superlattices, *Nature* **556**, 43 (2018).
- [3] M. Yankowitz, S. Chen, H. Polshyn, Y. Zhang, K. Watanabe, T. Taniguchi, D. Graf, A. F. Young, and C. R. Dean, Tuning superconductivity in twisted bilayer graphene, *Science* **363**, 1059 (2019).
- [4] X. Lu, P. Stepanov, W. Yang, M. Xie, M. A. Aamir, I. Das, C. Urgell, K. Watanabe, T. Taniguchi, G. Zhang, A. Bachtold, A. H. MacDonald, and D. K. Efetov, Superconductors, orbital magnets and correlated states in magic-angle bilayer graphene, *Nature* **574**, 653 (2019).
- [5] E. Y. Andrei and A. H. MacDonald, Graphene bilayers with a twist, *Nature Materials* **19**, 1265 (2020).
- [6] L. Balents, C. R. Dean, D. K. Efetov, and A. F. Young, Superconductivity and strong correlations in moiré flat bands, *Nature Physics* **16**, 725 (2020).
- [7] Y. Tang, L. Li, T. Li, Y. Xu, S. Liu, K. Barmak, K. Watanabe, T. Taniguchi, A. H. MacDonald, J. Shan, *et al.*, Simulation of hubbard model physics in  $wse_2/ws_2$  moiré superlattices, *Nature* **579**, 353 (2020).
- [8] E. C. Regan, D. Wang, C. Jin, M. I. B. Utama, B. Gao, X. Wei, S. Zhao, W. Zhao, Z. Zhang, K. Yumigeta, *et al.*, Mott and generalized wigner crystal states in  $wse_2/ws_2$  moiré superlattices, *Nature* **579**, 359 (2020).
- [9] O. Can, T. Tummuru, R. P. Day, I. Elfimov, A. Damascelli, and M. Franz, High-temperature topological superconductivity in twisted double-layer copper oxides, *Nature Physics* **17**, 519 (2021).
- [10] S. F. Zhao, X. Cui, P. A. Volkov, H. Yoo, S. Lee, J. A. Gardener, A. J. Akey, R. Engelke, Y. Ronen, R. Zhong, *et al.*, Time-reversal symmetry breaking superconductivity between twisted cuprate superconductors, *Science* **382**, 1422 (2023).
- [11] R. Bistritzer and A. H. MacDonald, Moiré bands in twisted double-layer graphene, *Proceedings of the National Academy of Sciences* **108**, 12233 (2011).
- [12] G. Tarnopolsky, A. J. Kruchkov, and A. Vishwanath, Origin of magic angles in twisted bilayer graphene, *Physical Review Letters* **122**, 106405 (2019).
- [13] F. Wu, A. H. MacDonald, and I. Martin, Theory of phonon-mediated superconductivity in twisted bilayer graphene, *Physical Review Letters* **121**, 257001 (2018).
- [14] H. Isobe, N. F. Yuan, and L. Fu, Unconventional superconductivity and density waves in twisted bilayer graphene, *Physical Review X* **8**, 041041 (2018).
- [15] B. Lian, Z. Wang, and B. A. Bernevig, Twisted bilayer graphene: A phonon-driven superconductor, *Physical Review Letters* **122**, 257002 (2019).
- [16] A. L. Sharpe, E. J. Fox, A. W. Barnard, J. Finney, K. Watanabe, T. Taniguchi, M. A. Kastner, and D. Goldhaber-Gordon, Emergent ferromagnetism near three-quarters filling in twisted bilayer graphene, *Science* **365**, 605 (2019).
- [17] J.-X. Lin, Y.-H. Zhang, E. Morissette, Z. Wang, S. Liu, D. Rhodes, K. Watanabe, T. Taniguchi, J. Hone, and J. I. A. Li, Spin-orbit-driven ferromagnetism at half moiré filling in magic-angle twisted bilayer graphene, *Science* **375**, 437 (2022).
- [18] E. M. Spanton, A. A. Zibrov, H. Zhou, T. Taniguchi, K. Watanabe, M. P. Zaletel, and A. F. Young, Observation of fractional chern insulators in a van der waals

- heterostructure, *Science* **360**, 62–66 (2018).
- [19] Y. Zeng, Z. Xia, K. Kang, J. Zhu, P. Knüppel, C. Vaswani, K. Watanabe, T. Taniguchi, K. F. Mak, and J. Shan, Thermodynamic evidence of fractional chern insulator in moiré mote<sub>2</sub>, *Nature* **622**, 69–73 (2023).
- [20] N. Morales-Durán, N. Wei, J. Shi, and A. H. MacDonald, Magic angles and fractional chern insulators in twisted homobilayer transition metal dichalcogenides, *Physical Review Letters* **132**, 096602 (2024).
- [21] C. Wang, X.-W. Zhang, X. Liu, Y. He, X. Xu, Y. Ran, T. Cao, and D. Xiao, Fractional chern insulator in twisted bilayer mote<sub>2</sub>, *Physical Review Letters* **132**, 036501 (2024).
- [22] Z. Liu and E. J. Bergholtz, Recent developments in fractional chern insulators, in *Encyclopedia of Condensed Matter Physics* (Elsevier, 2024) p. 515–538.
- [23] J. Cai, E. Anderson, C. Wang, X. Zhang, X. Liu, W. Holtzmann, Y. Zhang, F. Fan, T. Taniguchi, K. Watanabe, Y. Ran, T. Cao, L. Fu, D. Xiao, W. Yao, and X. Xu, Signatures of fractional quantum anomalous hall states in twisted mote<sub>2</sub>, *Nature* **622**, 63 (2023).
- [24] H. Park, J. Cai, E. Anderson, Y. Zhang, J. Zhu, X. Liu, C. Wang, W. Holtzmann, C. Hu, Z. Liu, T. Taniguchi, K. Watanabe, J.-H. Chu, T. Cao, L. Fu, W. Yao, C.-Z. Chang, D. Cobden, D. Xiao, and X. Xu, Observation of fractionally quantized anomalous hall effect, *Nature* **622**, 74 (2023).
- [25] F. Xu, Z. Sun, T. Jia, C. Liu, C. Xu, C. Li, Y. Gu, K. Watanabe, T. Taniguchi, B. Tong, J. Jia, Z. Shi, S. Jiang, Y. Zhang, X. Liu, and T. Li, Observation of integer and fractional quantum anomalous hall effects in twisted bilayer mote<sub>2</sub>, *Physical Review X* **13**, 031037 (2023).
- [26] Z. Lu, T. Han, Y. Yao, A. P. Reddy, J. Yang, J. Seo, K. Watanabe, T. Taniguchi, L. Fu, and L. Ju, Fractional quantum anomalous hall effect in multilayer graphene, *Nature* **626**, 759–764 (2024).
- [27] S. Carr, D. Massatt, S. Fang, P. Cazeaux, M. Luskin, and E. Kaxiras, Twistronics: Manipulating the electronic properties of two-dimensional layered structures through their twist angle, *Physical Review B* **95**, 075420 (2017).
- [28] S. Carr, S. Fang, and E. Kaxiras, Electronic-structure methods for twisted moiré layers, *Nature Reviews Materials* **5**, 748 (2020).
- [29] P. Wang, Y. Zheng, X. Chen, C. Huang, Y. V. Kartashov, L. Torner, V. V. Konotop, and F. Ye, Localization and delocalization of light in photonic moiré lattices, *Nature* **577**, 42 (2020).
- [30] B. Lou, B. Wang, J. A. Rodríguez, M. Cappelli, and S. Fan, Tunable guided resonance in twisted bilayer photonic crystal, *Science Advances* **8**, eadd4339 (2022).
- [31] H. Tang, B. Lou, F. Du, M. Zhang, X. Ni, W. Xu, R. Jin, S. Fan, and E. Mazur, Experimental probe of twist angle-dependent band structure of on-chip optical bilayer photonic crystal, *Science Advances* **9**, eadh8498 (2023).
- [32] H.-Y. Luan, Y.-H. Ouyang, Z.-W. Zhao, W.-Z. Mao, and R.-M. Ma, Reconfigurable moiré nanolaser arrays with phase synchronization, *Nature* **624**, 282 (2023).
- [33] Z. Meng, L. Wang, W. Han, F. Liu, K. Wen, C. Gao, P. Wang, C. Chin, and J. Zhang, Atomic bose-einstein condensate in twisted-bilayer optical lattices, *Nature* **615**, 231 (2023).
- [34] F. Wu, R.-X. Zhang, and S. Das Sarma, Three-dimensional topological twistronics, *Physical Review Research* **2**, 022010 (2020).
- [35] Z. Song, X. Sun, and L.-W. Wang, Eshelby-twisted three-dimensional moiré superlattices, *Physical Review B* **103**, 245206 (2021).
- [36] L. Xian, A. Fischer, M. Claassen, J. Zhang, A. Rubio, and D. M. Kennes, Engineering three-dimensional moiré flat bands, *Nano Letters* **21**, 7519–7526 (2021).
- [37] X. Lu, B. Xie, Y. Yang, Y. Zhang, X. Kong, J. Li, F. Ding, Z.-J. Wang, and J. Liu, Magic momenta and three-dimensional landau levels from a three-dimensional graphite moiré superlattice, *Physical Review Letters* **132**, 056601 (2024).
- [38] We note that previously we have implicitly assumes that we consider matrices on the field of real numbers. Thus, to avoid confusion, we shall denote SO(3) by SO(3, ℝ) hereafter.
- [39] See supplementary material for details.
- [40] C. Huang, F. Ye, X. Chen, Y. V. Kartashov, V. V. Konotop, and L. Torner, Localization-delocalization wavepacket transition in pythagorean aperiodic potentials, *Scientific Reports* **6**, 32546 (2016).
- [41] They are three  $C_4$  axes along the three perpendicular edges (such as the (100) direction) of the cube, four  $C_3$  axes along the body diagonals (such as (111)), and six  $C_2$  axes along the face diagonals (such as (110)).
- [42] M. Hirayama, R. Okugawa, S. Ishibashi, S. Murakami, and T. Miyake, Weyl node and spin texture in trigonal tellurium and selenium, *Physical Review Letters* **114**, 206401 (2015).
- [43] X. Zhang, L. Jin, X. Dai, and G. Liu, Topological type-ii nodal line semimetal and dirac semimetal state in stable kagome compound mg<sub>3</sub>bi<sub>2</sub>, *The Journal of Physical Chemistry Letters* **8**, 4814 (2017).
- [44] Q. Wu, C. Piveteau, Z. Song, and O. V. Yazyev, Mgta 2 n 3: A reference dirac semimetal, *Physical Review B* **98**, 081115 (2018).
- [45] G. Hua, S. Nie, Z. Song, R. Yu, G. Xu, and K. Yao, Dirac semimetal in type-iv magnetic space groups, *Physical Review B* **98**, 201116 (2018).
- [46] Y.-H. Chan, B. Kilic, M. M. Hirschmann, C.-K. Chiu, L. M. Schoop, D. G. Joshi, and A. P. Schnyder, Symmetry-enforced band crossings in trigonal materials: Accordion states and weyl nodal lines, *Physical Review Materials* **3**, 124204 (2019).
- [47] The codes are available at <https://github.com/physicswange/3D-Moire-Crystal>.
- [48] A. Burkov, M. Hook, and L. Balents, Topological nodal semimetals, *Physical Review B* **84**, 235126 (2011).
- [49] C. Fang, Y. Chen, H.-Y. Kee, and L. Fu, Topological nodal line semimetals with and without spin-orbital coupling, *Physical Review B* **92**, 081201 (2015).
- [50] R. Yu, H. Weng, Z. Fang, X. Dai, and X. Hu, Topological node-line semimetal and dirac semimetal state in antiperovskite Cu<sub>3</sub>PdN, *Physical Review Letters* **115**, 036807 (2015).
- [51] C. Fang, H. Weng, X. Dai, and Z. Fang, Topological nodal line semimetals, *Chinese Physics B* **25**, 117106 (2016).
- [52] Q. Xu, R. Yu, Z. Fang, X. Dai, and H. Weng, Topological nodal line semimetals in the CaP<sub>3</sub> family of materials, *Physical Review B* **95**, 045136 (2017).
- [53] B. Yan and C. Felser, Topological materials: Weyl semimetals, *Annual Review of Condensed Matter Physics* **8**, 337 (2017).
- [54] N. Armitage, E. Mele, and A. Vishwanath, Weyl and

- dirac semimetals in three-dimensional solids, *Reviews of Modern Physics* **90**, 015001 (2018).
- [55] K. Kim, A. DaSilva, S. Huang, B. Fallahazad, S. Larentis, T. Taniguchi, K. Watanabe, B. J. LeRoy, A. H. MacDonald, and E. Tutuc, Tunable moiré bands and strong correlations in small-twist-angle bilayer graphene, *Proceedings of the National Academy of Sciences* **114**, 3364–3369 (2017).
- [56] Y. Shimazaki, I. Schwartz, K. Watanabe, T. Taniguchi, M. Kroner, and A. Imamoğlu, Strongly correlated electrons and hybrid excitons in a moiré heterostructure, *Nature* **580**, 472–477 (2020).
- [57] L. Wang, E.-M. Shih, A. Ghiotto, L. Xian, D. A. Rhodes, C. Tan, M. Claassen, D. M. Kennes, Y. Bai, B. Kim, K. Watanabe, T. Taniguchi, X. Zhu, J. Hone, A. Rubio, A. N. Pasupathy, and C. R. Dean, Correlated electronic phases in twisted bilayer transition metal dichalcogenides, *Nature Materials* **19**, 861–866 (2020).
- [58] G. Chen, A. L. Sharpe, E. J. Fox, Y.-H. Zhang, S. Wang, L. Jiang, B. Lyu, H. Li, K. Watanabe, T. Taniguchi, Z. Shi, T. Senthil, D. Goldhaber-Gordon, Y. Zhang, and F. Wang, Tunable correlated chern insulator and ferromagnetism in a moiré superlattice, *Nature* **579**, 56–61 (2020).
- [59] X.-W. Luo and C. Zhang, Spin-twisted optical lattices: Tunable flat bands and larkin-ovchinnikov superfluids, *Physical Review Letters* **126**, 103201 (2021).
- [60] L. Lu, Z. Wang, D. Ye, L. Ran, L. Fu, J. D. Joannopoulos, and M. Soljačić, Experimental observation of weyl points, *Science* **349**, 622 (2015).
- [61] Y. Zhang, F. Zhang, Z. Yan, Q. Ma, X. Li, Y. Huang, and J. A. Rogers, Printing, folding and assembly methods for forming 3d mesostructures in advanced materials, *Nature Reviews Materials* **2**, 1 (2017).
- [62] Y. Yang, Z. Gao, H. Xue, L. Zhang, M. He, Z. Yang, R. Singh, Y. Chong, B. Zhang, and H. Chen, Realization of a three-dimensional photonic topological insulator, *Nature* **565**, 622 (2019).